Translational Science

Cancer Research

Targeting Glycolysis through Inhibition of Lactate Dehydrogenase Impairs Tumor Growth in Preclinical Models of Ewing Sarcoma

Choh Yeung[1], Anna E. Gibson[1], Sameer H. Issaq[1], Nobu Oshima[2], Joshua T. Baumgart[1], Leah D. Edessa[1], Ganesha Rai[3], Daniel J. Urban[3], Michelle S. Johnson[4], Gloria A. Benavides[4], Giuseppe L. Squadrito[4], Marielle E. Yohe[1], Haiyan Lei[1], Sandy Eldridge[5], John Hamre III[6], Tyrone Dowdy[7], Victor Ruiz-Rodado[7], Adrian Lita[7], Arnulfo Mendoza[1], Jack F. Shern[1], Mioara Larion[7], Lee J. Helman[1], Gordon M. Stott[8], Murali C. Krishna[9], Matthew D. Hall[3], Victor Darley-Usmar[4], Leonard M. Neckers[2], and Christine M. Heske[1]

Abstract

Altered cellular metabolism, including an increased dependence on aerobic glycolysis, is a hallmark of cancer. Despite the fact that this observation was first made nearly a century ago, effective therapeutic targeting of glycolysis in cancer has remained elusive. One potentially promising approach involves targeting the glycolytic enzyme lactate dehydrogenase (LDH), which is overexpressed and plays a critical role in several cancers. Here, we used a novel class of LDH inhibitors to demonstrate, for the first time, that Ewing sarcoma cells are exquisitely sensitive to inhibition of LDH. EWS-FLI1, the oncogenic driver of Ewing sarcoma, regulated LDH A (LDHA) expression. Genetic depletion of LDHA inhibited proliferation of Ewing sarcoma cells and induced apoptosis, phenocopying pharmacologic inhibition of LDH. LDH inhibitors affected Ewing sarcoma cell viability both *in vitro* and *in vivo* by reducing glycolysis. Intravenous administration of LDH inhibitors resulted in the greatest intratumoral drug accumulation, inducing tumor cell death and reducing tumor growth. The major dose-limiting toxicity observed was hemolysis, indicating that a narrow therapeutic window exists for these compounds. Taken together, these data suggest that targeting glycolysis through inhibition of LDH should be further investigated as a potential therapeutic approach for cancers such as Ewing sarcoma that exhibit oncogene-dependent expression of LDH and increased glycolysis.

Significance: LDHA is a pharmacologically tractable EWS-FLI1 transcriptional target that regulates the glycolytic dependence of Ewing sarcoma.

Introduction

Glycolytic dependence of cancer cells was first described in 1927 by Otto Warburg, who hypothesized that tumor cells preferentially catabolized glucose to lactate even in the presence of oxygen (aerobic glycolysis), whereas normal cells preferentially catabolized glucose to carbon dioxide (oxidative phosphorylation; ref. 1). Targeting this increased dependence on glycolysis in cancer cells presents an opportunity to inhibit their growth while potentially limiting the toxicity delivered to normal cells (2). Since this initial discovery, our understanding of these processes has evolved to reflect the role of genetic alterations in cancer cells, including the activation of genes, such as lactate dehydrogenase A (LDHA), the enzyme responsible for the conversion of pyruvate to lactate, the final enzymatic step in the glycolytic pathway (3). Several studies have shown that LDHA plays a key role in tumor initiation and maintenance, and that inhibition of LDHA reduces cellular growth and metastasis in preclinical cancer models (4–9). Intriguingly, many glycolytic tumors display elevated levels of

[1]Pediatric Oncology Branch, National Cancer Institute, National Institutes of Health, Bethesda, Maryland. [2]Urologic Oncology Branch, National Cancer Institute, National Institutes of Health, Bethesda, Maryland. [3]Chemical Genomics Center, National Center for Advancing Translational Sciences, National Institutes of Health, Rockville, Maryland. [4]Mitochondrial Medicine Laboratory, Department of Pathology, University of Alabama at Birmingham, Birmingham, Alabama. [5]Division of Cancer Treatment and Diagnosis, National Cancer Institute, National Institutes of Health, Bethesda, Maryland. [6]Laboratory of Investigative Toxicology, Frederick National Laboratory for Cancer Research, Frederick, Maryland. [7]Neuro-Oncology Branch, National Cancer Institute, National Institutes of Health, Bethesda, Maryland. [8]Leidos Biomedical Research, Inc., Frederick National Laboratory for Cancer Research, Frederick, Maryland. [9]Radiation Biology Branch, National Cancer Institute, National Institutes of Health, Bethesda, Maryland.

Note: Supplementary data for this article are available at Cancer Research Online (http://cancerres.aacrjournals.org/).

Current address for S.H. Issaq: Urologic Oncology Branch, National Cancer Institute, National Institutes of Health, Bethesda, Maryland; and current address for L.J. Helman: Departments of Pediatrics and Medicine, Keck School of Medicine, University of Southern, California, Los Angeles, California and Children's Center for Cancer and Blood Diseases, Children's Hospital Los Angeles, Los Angeles, California.

Corresponding Author: Christine M. Heske, National Cancer Institute, 10 Center Drive, CRC, Room 1W-3816, Bethesda, MD 20892. Phone: 240-760-6197; Fax: 301-451-7010; E-mail: Christine.heske@nih.gov

Cancer Res 2019;79:5060–73

doi: 10.1158/0008-5472.CAN-19-0217

LDHA, and it appears to be expressed primarily in cancer cells, as opposed to normal tissues (10, 11). LDHA is therefore used as a biomarker for many malignancies (11) and is a promising target for cancer therapeutics.

To date, much of the data on LDH inhibition has been generated through proof-of-principle genetic studies that reveal LDHA knockdown inhibits *in vitro* and *in vivo* growth of certain cancer cell lines (4–7, 9). Although novel LDH inhibitors (LDHi) have been described, there are numerous issues with evaluating their translational potential, including suboptimal selectivity, potency, cellular permeability, and pharmacokinetic properties (4, 5, 12–14). Hence, the potential clinical applications of LDHi remain unrealized. Recently, renewed efforts have been made to more efficiently target LDH with agents developed through the National Cancer Institute Experimental Therapeutics (NExT) Program, a consortium that aims to develop drugs for difficult targets (15). NCI-737 and NCI-006 represent two novel LDHi that were developed and validated as part of the NExT Program.

In this study, we sought to evaluate the activity of NCI-737 and NCI-006, and to describe the impact of genetic and pharmacologic inhibition of LDH on cellular metabolism, growth, and survival on *in vitro* and *in vivo* preclinical models of Ewing sarcoma. Ewing sarcoma is an aggressive malignancy of the bones and soft tissues that primarily affects adolescents and young adults and is driven by a reciprocal oncogenic translocation between *EWSR1* and an *ETS* family member such as *FLI1* or *ERG* that results in aberrant gene expression (16–18). Ewing sarcoma remains a disease for which new therapies are critically needed, given that outcomes for high-risk patients remain poor and have not improved in decades (19–21). In this study, we show that Ewing sarcoma cells are exquisitely sensitive to inhibition of LDH activity, both genetically and pharmacologically. Further, glycolytic inhibition with either NCI-006 or NCI-737 impairs growth and survival of Ewing sarcoma *in vitro* and *in vivo*.

Materials and Methods

Compounds

NCI-737 and NCI-006, equipotent against LDHA and LDHB, were obtained through the NExT Program (15). Details of compounds and their synthesis can be found in Supplementary Methods. Stock solutions for *in vitro* use were prepared in DMSO, aliquoted, and stored at -20°C. For *in vivo* use, powdered compound was dissolved in a volume of 0.1N NaOH, equivalent to 18% of the total solution volume, and added to PBS. Dropwise addition of 1N HCl was performed to achieve a pH of 7.4 to 7.8. Solution was prepared weekly and kept at 4°C.

Cell line screen

The cell line screen was performed by Oncolead using a panel of 94-cell lines and a 72-hour sulforhodamine assay.

Cell lines

Ewing sarcoma cell lines TC32, TC71, EW8, and RDES have been previously described (2). SK-N-MC and CHLA-258 were obtained from Dr. Lee Helman (Children's Hospital of Los Angeles, Los Angeles, CA). 5838 was obtained from the ATCC. Cell lines were authenticated by short tandem repeat DNA fingerprinting and compared with known sequences. TC32 (RRID: CVCL_7151), TC71 (RRID: CVCL_2213), EW8 (RRID: CVCL_V618), and CHLA-258 (RRID: CVCL_A058) were most recently authenticated in 2018 in the lab of Dr. Stephen Channock (National Cancer Institute, Rockville, MD). SK-N-MC (RRID: CVCL_0530) and RDES (RRID: CVCL_2169) were most recently authenticated in 2012 by Genetica Cell Line Testing. 5838 (RRID: CVCL_6255) has not been independently authenticated since purchase from the ATCC.

Mycoplasma testing of these cell lines was most recently performed in January 2019 and confirmed negative results. Experiments were performed on cells that were passaged between 5 and 12 times.

Cells were maintained in RPMI growth medium (Life Technologies) with 10% FBS (Sigma Aldrich), 100 U/mL penicillin and 100 μg/mL streptomycin (Life Technologies), and 2 mmol/L L-glutamine (Life Technologies) at 37°C in an atmosphere of 5% CO_2.

Cell proliferation assays

Cellular proliferation was monitored in real-time using the IncuCyte live cell analysis system (Essen BioScience), and cellular viability was determined by MTT assay (Promega) according to the manufacturer's instructions. For both methods, cells were plated at a density of 2,000 cells/well in 96-well plates overnight and treated the following day.

Protein analysis

Cell lysates were prepared by plating 1 million cells/10-cm plate overnight and then treating cells for an additional 24 hours. Cells were harvested with 1X RIPA (Santa Cruz Biotechnology) plus phosphatase and protease inhibitor cocktail (ThermoFisher). Protein lysates (30 μg/lane) were quantified by BCA protein assay (ThermoFisher). Blots were prepared as previously described (22) and incubated with primary antibodies, as described in Supplementary Methods.

Flow cytometry

Cells were plated at 1 million cells/10-cm plate and treated the following day. Cells were harvested using PBS-based, enzyme-free cell dissociation buffer (Life Technologies) at 72 hours and processed according to the Annexin V–FITC apoptosis detection kit (Sigma), before being run through the LSR Fortessa flow cytometer (BD Biosciences).

siRNA studies

Lipofectamine RNAi Max (ThermoFisher) was used according to the manufacturer's instructions. Additional details of siRNA sequences and experimental conditions can be found in Supplementary Methods.

Chromatin immunoprecipitation sequencing analysis

FASTQ files from published FLI1 and H3K27ac chromatin immunoprecipitation sequencing (ChIP-seq), as well as associated RNA-seq experiments, were downloaded from NCI GEO (GSE8826 and GSE89026). Reads were aligned to the hg19 reference genome using BWA (version 0.7.10) using an established pipeline (23). Resulting tdf files were visualized using IGV (version 2.3.40).

Biochemical analyses

The YSI 2950D Biochemistry Analyzer (Xylem Inc.) was used to measure glucose and lactate in the media of cells treated with

NCI-737 (187 nmol/L) or DMSO (control). Cells were plated in triplicate in 24-well plates as follows: 500,000 cells/well for TC71 and EW8, 600,000 cells/well for RDES, and 250,000 cells/well for TC32. Media were collected after 24 hours of treatment, and the plate with cells was frozen at -80°C and subsequently lysed with 1X RIPA buffer (Santa Cruz Biotechnology) for protein assay.

Pyruvate assay

Intracellular pyruvate concentrations were determined using the Pyruvate Assay Kit (Abcam). Cells were plated at 2 million/10-cm plate and treated with 187 nmol/L NCI-737 for 24 hours. Cells were lysed using 200 μL pyruvate sample buffer. Proteins were precipitated from the lysate with perchloric acid and neutralized with KOH according to the manufacturer's instructions. Pyruvate was measured using the fluorometric assay protocol.

NAD^+/NADH assay

Five thousand cells/well were plated in ViewPlate-96 96-well microplates (PerkinElmer) and treated with up to 187 nmol/L of NCI-737 for 13 hours. NAD^+/NADH ratio was determined using the NAD^+/NADH-Glo assay (Promega) according to the manufacturer's instructions.

Extracellular flux analysis

Analyses of cellular bioenergetics were performed using the Seahorse XF^e96 Extracellular Flux Analyzer (Agilent). Glycolytic stress tests were performed according to the manufacturer's instructions, as previously described (24, 25). Additional experimental details can be found in Supplementary Methods.

LDH activity assay

Cells were plated overnight at 200,000 cells/well in 24-well plates. The following morning, cells were acclimated to XF complete media for 30 minutes prior to treatment with the indicated concentrations of LDHi or DMSO (control) for 1 hour (dose–response experiment) at 37°C in a non-CO_2 incubator. For the time-point experiment, cells were incubated in XF complete media with the LDHi for the indicated time points. Cells were lysed using 100 μL LDH assay buffer and the oxidation of NADH measured spectrophotometrically at 340 nm.

^{13}C-Glucose tracing

Details of sample preparation for liquid chromatography mass spectrometry and nuclear magnetic resonance analyses can be found in Supplementary Methods. Liquid chromatography mass spectrometry analysis has been previously described (26), but further details of this and nuclear magnetic resonance analysis can be found in Supplementary Methods.

Statistical analyses

Statistical significance was determined by two-tailed Student *t* test. $P < 0.05$ was considered significant.

In vivo studies

Animal studies were approved by and performed in accordance with the National Institutes of Health Animal Care and Use Committee guidelines. For all experiments described, female Fox Chase SCID beige mice (CB17.B6-Prkdcscid Lystbg/Crl) were purchased from Charles River Laboratories. Two million cells in a solution of Hank's Balanced Salt Solution were injected orthotopically into the gastrocnemius muscle in the left hind leg of each mouse. Mice were randomized when palpable tumors developed, at which point treatment with agents began. Specific details for each set of experimental conditions may be found in Supplementary Methods.

Statistical analyses

Tumor volumes were compared between groups using a two-tailed Student *t* test at serial time points. $P < 0.05$ was considered significant. Measurements for mice that had already reached endpoint were carried forward until all mice in the group had reached endpoint.

Histopathology and image analysis

Hematoxylin and eosin–stained slides were scanned using the Aperio XT ScanScope whole slide imaging system with a 20X objective lens (Aperio). One whole slide image (SVS file) was prepared from each animal, capturing the entire tumor section on the slide. Details of image analysis can be found in Supplementary Methods.

Hyperpolarized MRS

Hyperpolarized ^{13}C-MRI study was performed as described previously (27). Additional experimental details can be found in Supplementary Methods.

Intratumoral drug measurement

Measurement of tumor concentrations of LDHi was done by mass spectrometric analysis with internal standards (pure NCI-737 and NCI-006) and was performed by Quintara Discovery.

Intratumoral LDH activity measurement

Frozen tumor sections were pulverized in a liquid nitrogen–cooled pestle-mortar apparatus. Pulverized tumors were lysed in 10 volumes of LDH assay buffer and LDH activity measured as described above.

Results

Ewing sarcoma cells are sensitive to genetic and pharmacologic inhibition of LDHA, which decreases cellular proliferation and activates apoptotic pathways

To evaluate the functional activity of NCI-737 and NCI-006, we screened a panel of 94 cancer cell lines using the Oncolead cell panel assay, which represents a diverse array of cancer cell lines. Across this panel, Ewing sarcoma cell lines emerged among the top 10 and top 12 most sensitive cell lines to NCI-006 and NCI-737, respectively, with IC_{50} values of 100 to 200 nmol/L (median IC_{50} values for all cell lines in the panel were 1,260 nmol/L for NCI-006 and 845 nmol/L for NCI-737; Fig. 1A). Of note, other pediatric-type sarcoma cell lines (rhabdomyosarcoma and osteosarcoma) in the panel had median IC_{50} values in line with the general panel (1,037 nmol/L and 712 nmol/L, for NCI-006 and NCI-737, respectively; Supplementary Table S1). To validate these findings, additional *in vitro* studies of cellular viability were performed on a broader panel of Ewing sarcoma cell lines. By MTT assay, all Ewing sarcoma cell lines displayed nearly identical dose-dependent sensitivity to NCI-737 and NCI-006, with IC_{50} values ranging from 100 nmol/L (TC71 and TC32) to 1 μmol/L (RDES and EW8) for each compound at 72 hours of treatment (Supplementary Fig. S1A). Given the potential for metabolic inhibitors to affect reagents in this assay, we verified these findings using IncuCyte live cell analysis, which confirmed that both

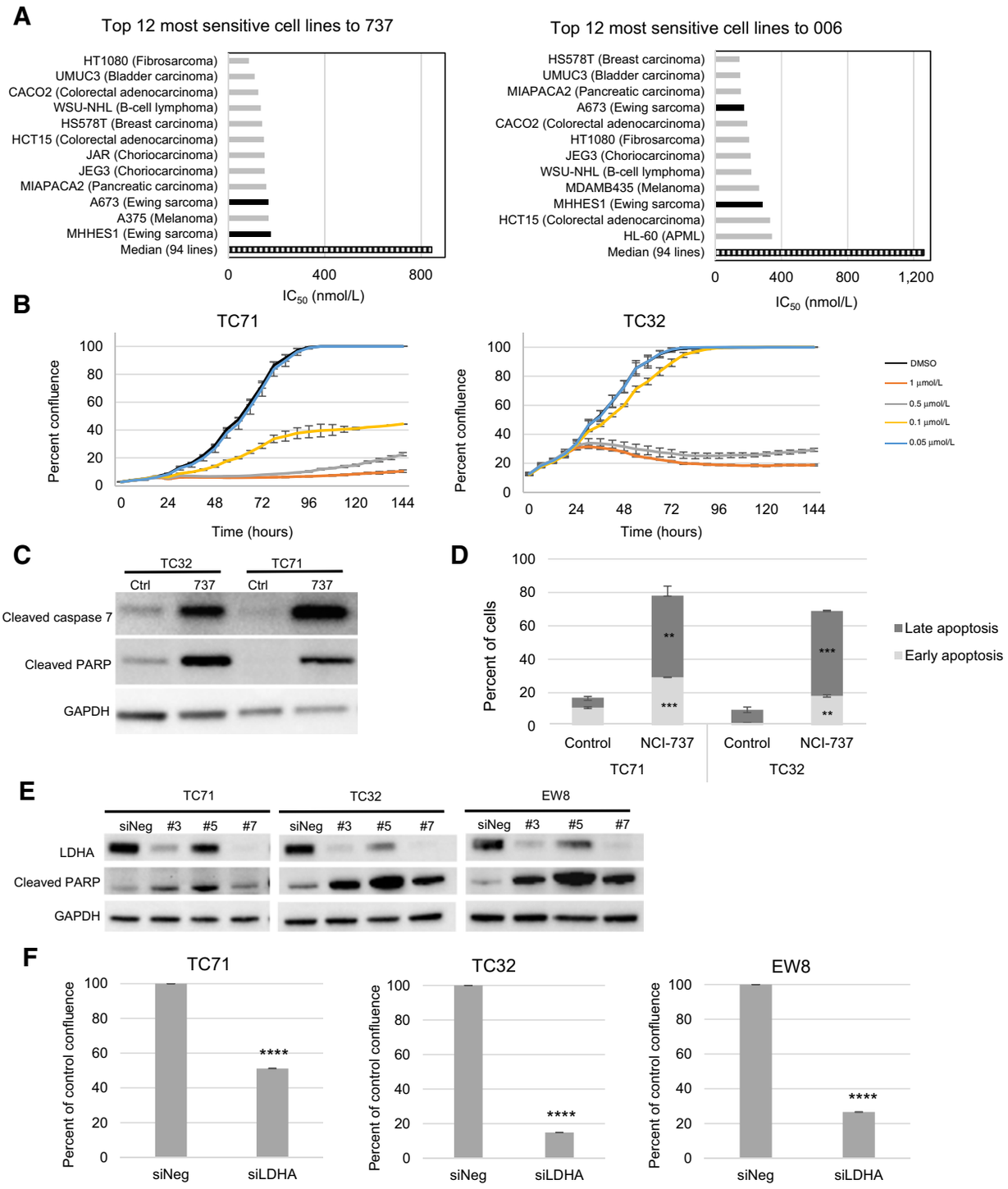

Figure 1.

Ewing sarcoma cells are sensitive to inhibition or loss of LDH activity. **A,** Relative IC_{50} values for top 12 most sensitive cell lines to LDHi NCI-737 and NCI-006, compared with median IC_{50} for 94 cancer cell lines (striped bar) tested in the Oncolead cell panel assay. Ewing sarcoma cell lines MHHES1 and A673 are shown in black. **B,** IncuCyte live-cell analysis of Ewing sarcoma cell lines TC71 and TC32 treated with NCI-737 at doses between 0.05 and 1 µmol/L, 24 hours after plating. **C,** Western blot analysis of Ewing sarcoma cell lines TC32 and TC71 with and without treatment with 1 µmol/L NCI-737 for 24 hours. **D,** Percentage of TC71 and TC32 cells in early apoptosis (Annexin V–positive, PI-negative) and late apoptosis (Annexin V–positive, PI-positive) with and without treatment with 1 µmol/L NCI-737 for 72 hours, measured by flow cytometry. **E,** Western blot analysis of LDHA and cleaved PARP in EWS cell lines (TC71, TC32, and EW8) 72 hours after LDHA siRNA knockdown. **F,** Relative viability of Ewing sarcoma cells (TC71, TC32, and EW8) following knockdown with siLDHA sequence #5 for 72 hours, expressed as percentage of control confluence ± SEM. **, $P < 0.01$; ***, $P < 0.001$; ****, $P < 0.0001$, as compared with control.

NCI-737 and NCI-006 inhibited cellular proliferation at doses in the 100–500 nmol/L range across multiple cell lines (Fig. 1B; Supplementary Fig. S1B and S1C). Notably, the IC_{50} values for each of the compounds were very similar for each cell line tested, indicating equal potency of NCI-737 and NCI-006 in the Ewing sarcoma cell line models.

To evaluate the mechanisms behind this loss of viability, we performed Western blot analysis of cells treated with NCI-737, which revealed activation of proapoptotic proteins, cleaved PARP, and cleaved caspase 7 at 24 hours (Fig. 1C). Flow cytometry analysis of Ewing sarcoma cells treated with NCI-737 for 72 hours demonstrated a significant increase in the percentage of cells in both early and late apoptosis (Fig. 1D). Taken together, these findings suggest that the observed decrease in Ewing sarcoma cellular proliferation caused by LDHi is due to apoptotic cell death.

Next, we examined the result of genetic loss of LDHA and LDHB in Ewing sarcoma cell lines by knocking down the enzymes using siRNA to determine whether the results of pharmacologic LDH inhibition would be recapitulated. *LDHA* knockdown resulted in the expected loss of LDHA protein in Ewing sarcoma cell lines. As with the LDHi, genetic knockdown of *LDHA* resulted in decreased cellular proliferation and induction of apoptotic markers (Fig. 1E and F; Supplementary Fig. S2A and S2B), consistent with the conclusion that LDHA is important for Ewing sarcoma cell survival. In contrast, knockdown of *LDHB* with four siRNA sequences in multiple cell lines neither induced apoptosis nor negatively affected proliferation of Ewing sarcoma cells (Supplementary Fig. S2C–S2E).

LDHA is regulated by EWS-FLI1

Ewing sarcoma is characterized by a reciprocal translocation between chromosomes 11 and 22, resulting in the oncogenic transcription factor EWS-FLI1, which acts as the primary driver of the disease (17, 18). Although attempts to target EWS-FLI1 directly have yet to yield an effective therapeutic, examining the downstream effects of EWS-FLI1 has the potential to reveal insights into Ewing sarcoma biology that may be translated in clinically meaningful ways (28, 29). Given the marked sensitivity to both genetic depletion and pharmacologic inhibition of LDHA in Ewing sarcoma cells, as well as the recent findings that EWS-FLI1 regulates a shift away from oxidative metabolism toward glycolysis, which is NAD^+-dependent (30, 31), we sought to determine whether EWS-FLI1 might play a role in the regulation of *LDHA* and/or *LDHB*. Depletion of EWS-FLI1 with multiple siRNA sequences resulted in a decrease in LDHA protein, as well as a decrease in NROB1 protein, a known direct target of EWS-FLI1, in each of the four Ewing sarcoma cell lines tested (Fig. 2A; Supplementary Fig. S3A), suggesting that LDHA expression is regulated, at least in part, by EWS-FLI1. In contrast, depletion of EWS-FLI1 had no effect on LDHB expression in each of the four Ewing sarcoma cell lines tested (Supplementary Fig. S3B).

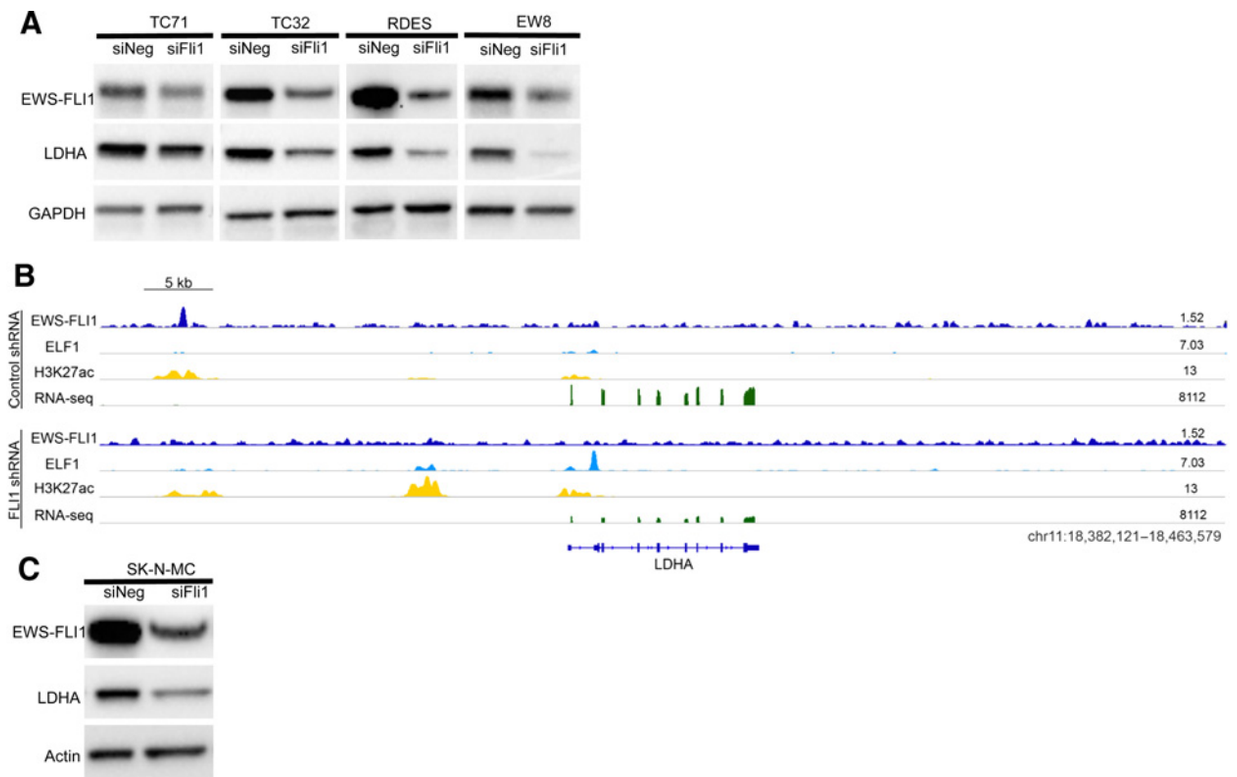

Figure 2.
EWS-FLI1 regulates LDHA expression. **A,** Western blot analysis of EWS-FLI1 and LDHA 72 hours following EWS-FLI1 siRNA knockdown with sequence #8 in Ewing sarcoma cell lines (TC71, TC32, RDES, and EW8). **B,** Representative ChIP-seq tracks for EWS-FLI1 (dark blue), ELF1 (light blue), and H3K24ac (yellow) from SK-N-MC Ewing sarcoma cells expressing either control shRNA (top) or EWS-FLI1 shRNA (bottom). RNA-seq tracks at the *LDHA* locus are shown for each cell line (green). **C,** Western blot analysis of LDHA protein level in SK-N-MC cells 72 hours following EWS-FLI1 siRNA knockdown with sequence #8.

To evaluate whether *LDHA* might be a direct EWS-FLI1 target, we examined publicly available ChIP-seq data generated using the shFLI1-transfected Ewing sarcoma cell line SK-N-MC (32). In the FLI1 knockdown, EWS-FLI1 and H3K27-acetylation deposition at the *LDHA* locus were decreased, and a corresponding decrease in *LDHA* mRNA expression was observed (Fig. 2B). An expected decrease in LDHA protein with EWS-FLI1 depletion in SK-N-MC was similarly observed (Fig. 2C). Furthermore, an analysis of publicly available ChIP-seq data on primary Ewing sarcoma tumors (33) also demonstrated H3K27ac deposition at the *LDHA* enhancer (Supplementary Fig. S3C). Analysis of ChIP-seq data from the same shFLI1-transfected Ewing sarcoma cell line SK-N-MC revealed that there was neither EWS-FLI1 nor H3K27-acetylation present at the *LDHB* locus (Supplementary Fig. S3D). Similarly, there was no change in LDHB protein with EWS-FLI1 depletion in this cell line (Supplementary Fig. S3E). Collectively, these data suggest that *LDHA*, but not *LDHB*, is a direct target of EWS-FLI1, and supports further investigation of the translational potential of pharmacologic LDH inhibition in Ewing sarcoma.

LDHi act through impairment of glycolysis in Ewing sarcoma cells

To evaluate on-target activity of these LDHi, we characterized the enzymatic inhibition and downstream metabolic effects of these agents. First, we assessed expression levels of LDHA and LDHB, and baseline LDH activity level in Ewing sarcoma cell lines, and determined there was uniform expression and enzymatic activity across the panel (Supplementary Fig. S4A and S4B). Next, we examined the change in basal LDH activity with increasing doses of NCI-737 or NCI-006 and found a dose-dependent inhibition of LDH activity in Ewing sarcoma cell lines for each of the compounds (Fig. 3A). For each of the cell lines tested (TC71, TC32, and EW8), the IC_{50} values for LDH inhibition were similar for both agents, at approximately 100 nmol/L, consistent with the observation that LDH appears to be uniformly expressed and active in these cell lines. Notably, the LDHi resulted in rapid inhibition of LDH upon exposure to Ewing sarcoma cells, with LDH activity decreasing within 30 seconds of drug exposure and reaching maximal inhibition by approximately 10 minutes *in vitro* (Supplementary Fig. S4C).

Next, biochemical analyses of glucose and lactate content in the culture media of treated and untreated cells were performed using YSI analysis and demonstrated a significant decrease in glucose consumption and lactate production in four Ewing sarcoma cell lines treated with NCI-737 (Fig. 3B). Furthermore, LDHi treatment induced an increase in intracellular pyruvate concentration in all four cell lines (Fig. 3C). Confirmatory biochemical studies, performed using mass spectrometry–based analysis of intracellular pools of pyruvate and lactate in Ewing sarcoma cells treated with LDHi, demonstrated a similar increase in steady-state levels of pyruvate and a decrease in steady-state levels of lactate in Ewing sarcoma cells treated with NCI-737 (Supplementary Fig. S5A and S5B).

We next examined the impact of LDHi treatment on trace labeling of intracellular pyruvate pools and lactate release using ^{13}C-labeled glucose. In both Ewing sarcoma cell lines tested, we observed a significant increase in accumulation of ^{13}C-labeled intracellular pyruvate (M+3) after 6 hours of treatment with NCI-737 (Supplementary Fig. S5C and S5D). We also noted a significant decrease in the amount of ^{13}C-labeled lactate released into the media of treated cells, consistent with the data generated by YSI analysis (Supplementary Fig. S5E). Taken together, these data are consistent with NCI-737–mediated inhibition of LDH, resulting in accumulation of pyruvate that cannot be converted to lactate, resulting in a reduction of overall glucose consumption.

Because LDH is a major cytosolic regulator of redox homeostasis, we next examined the effect of NCI-737 on the cellular NAD^+/NADH ratio. Treatment with NCI-737 resulted in a dose-dependent decrease in the NAD^+/NADH ratio in all four Ewing sarcoma cell lines tested, compared with control (Fig. 3D), indicating that loss of NAD^+/NADH homeostasis is a key outcome of treatment with these LDHi.

To further understand the bioenergetic effects of LDH inhibition on Ewing sarcoma cells, we utilized extracellular flux analysis to perform a glycolytic stress test (24, 25) on cells treated with NCI-737 to examine changes in extracellular acidification rate (ECAR). In both TC71 and TC32 cell lines, NCI-737 treatment for 6 hours resulted in a dose-dependent decrease in both glycolysis (change in ECAR upon glucose addition) and glycolytic capacity (change in ECAR upon oligomycin treatment), with the effect on glycolytic capacity being more pronounced (Fig. 3E; Supplementary Fig. S6A). Notably, upon stimulation of glycolysis by addition of oligomycin, untreated cells were able to increase ECAR, whereas this effect was blunted or lost completely in cells treated with NCI-737. A comparison of the effects of NCI-006 with those of NCI-737 on glycolytic flux demonstrated that the two agents inhibited ECAR in a nearly identical manner across a range of doses (Supplementary Fig. S6B).

In addition, we examined the effect of short-term NCI-737 treatment on oxidative phosphorylation by measuring the oxygen consumption rate (OCR) of Ewing sarcoma cells. When treated with NCI-737 at doses that affected ECAR, no changes in OCR were observed in Ewing sarcoma cells (Supplementary Fig. S7A and S7B). Further, when cells were exposed to higher doses of LDHi, concentrations between 10 and 30 μmol/L were required to produce a decrease in OCR, whereas decreases in ECAR were noted at concentrations starting at less than 1 μmol/L (Supplementary Fig. S7C and S7D). Taken together with the proliferation data, these findings suggest that at doses under 10 μmol/L these LDHi induce metabolic changes within the glycolytic pathway that directly affect the ability of the cells to proliferate and survive.

Pharmacologic effects on bioenergetics predict effect on proliferation *in vitro*

Although all Ewing sarcoma cell lines tested exhibited sensitivity to LDHi, there were slight differences noted in the degree of the antiproliferative effects. To understand the basis for this differential sensitivity, we interrogated the Ewing sarcoma cell lines for differences in various characteristics. As previously described, no correlations were noted between cell line sensitivity to LDHi and basal LDH activity, LDHA or LDHB expression, basal glucose consumption, basal pyruvate level, or basal NAD^+/NADH ratio (Fig. 3B and D; Supplementary Fig. S4A and S4B). We did observe that the more sensitive cell lines had higher basal lactate production and a greater change in NAD^+/NADH ratios upon drug treatment, suggesting that LDH may play a greater role in maintaining the redox balance in sensitive cells (Fig. 3B and D). In addition, further evaluation of extracellular flux data revealed a dose-dependent decrease in both glycolysis (Supplementary Fig. S8A) and glycolytic capacity (Supplementary Fig. S8B) in all cell lines tested, with the extent of change for each parameter varying across the cell lines (Fig. 4A and B). For example, when

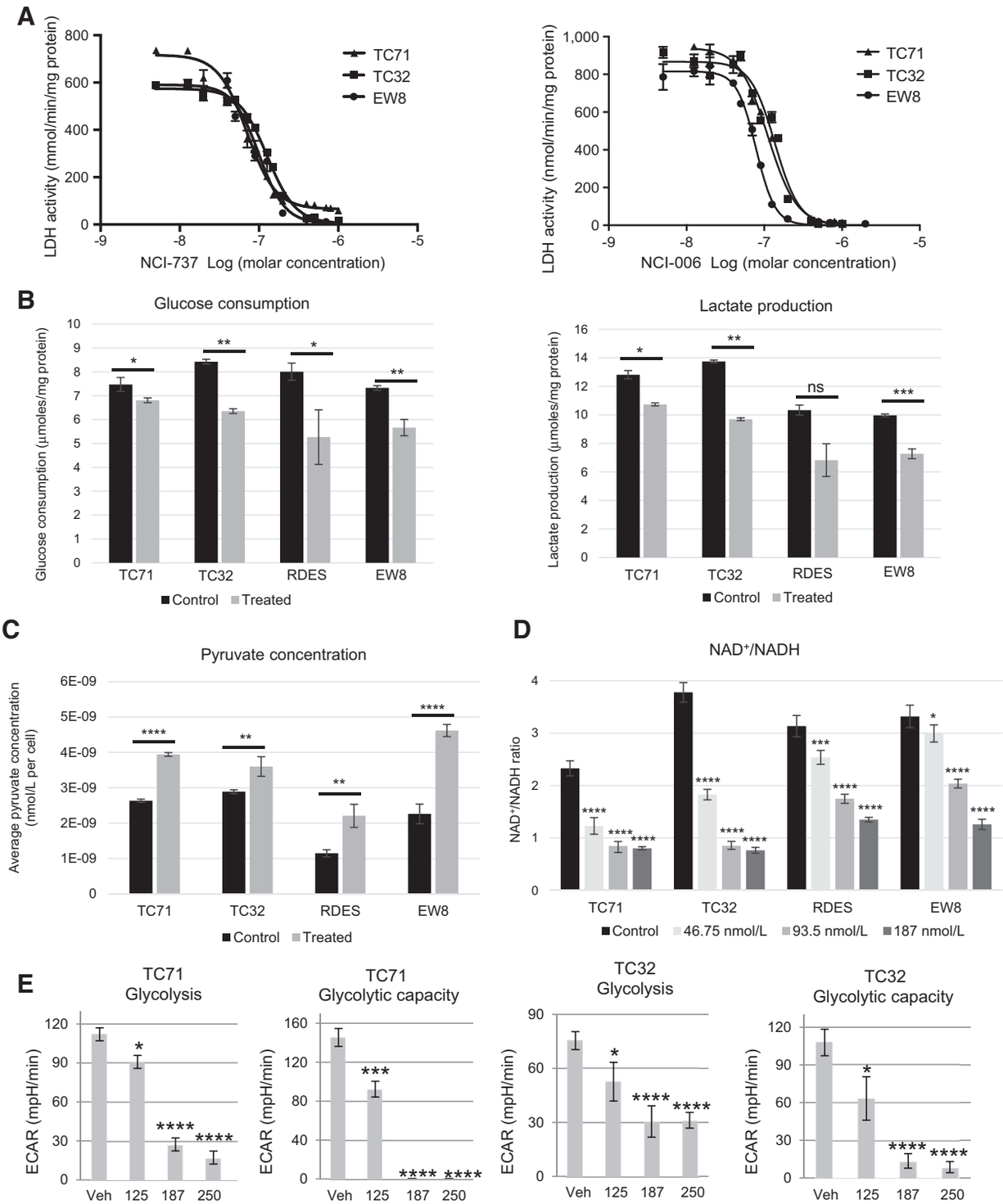

Figure 3.

LDHi act through impairment of glycolysis in Ewing sarcoma. **A,** Dose–response curves for change in LDH activity with increasing doses of NCI-737 or NCI-006 in Ewing sarcoma cell lines (TC71, TC32, and EW8). **B,** YSI analysis of glucose consumption and lactate production in Ewing sarcoma cells 24 hours after treatment with 187 nmol/L NCI-737. *P* values between groups: *, $P < 0.05$; **, $P < 0.01$; ***, $P < 0.001$. **C,** Intracellular pyruvate concentration in Ewing sarcoma cells 24 hours after treatment with 187 nmol/L NCI-737. *P* values between groups: **, $P < 0.001$; ****, $P < 0.0001$. **D,** NAD^+/NADH ratio in Ewing sarcoma cells treated with various doses of NCI-737 at 13 hours. *P* values, as compared with controls: *, $P < 0.05$; ***, $P < 0.001$; ****, $P < 0.0001$. **E,** Extracellular flux analysis was used to perform glycolytic stress tests of TC71 and TC32 cells treated with increasing doses of NCI-737. Glycolysis time-point indicates flux after glucose addition; glycolytic capacity time-point indicates flux after oligomycin addition. The *x*-axis reflects NCI-737 dose in nmol/L. Error bars, SD. *P* values, as compared with controls: *, $P < 0.05$; ***, $P < 0.001$; ****, $P < 0.0001$. ns, nonsignificant.

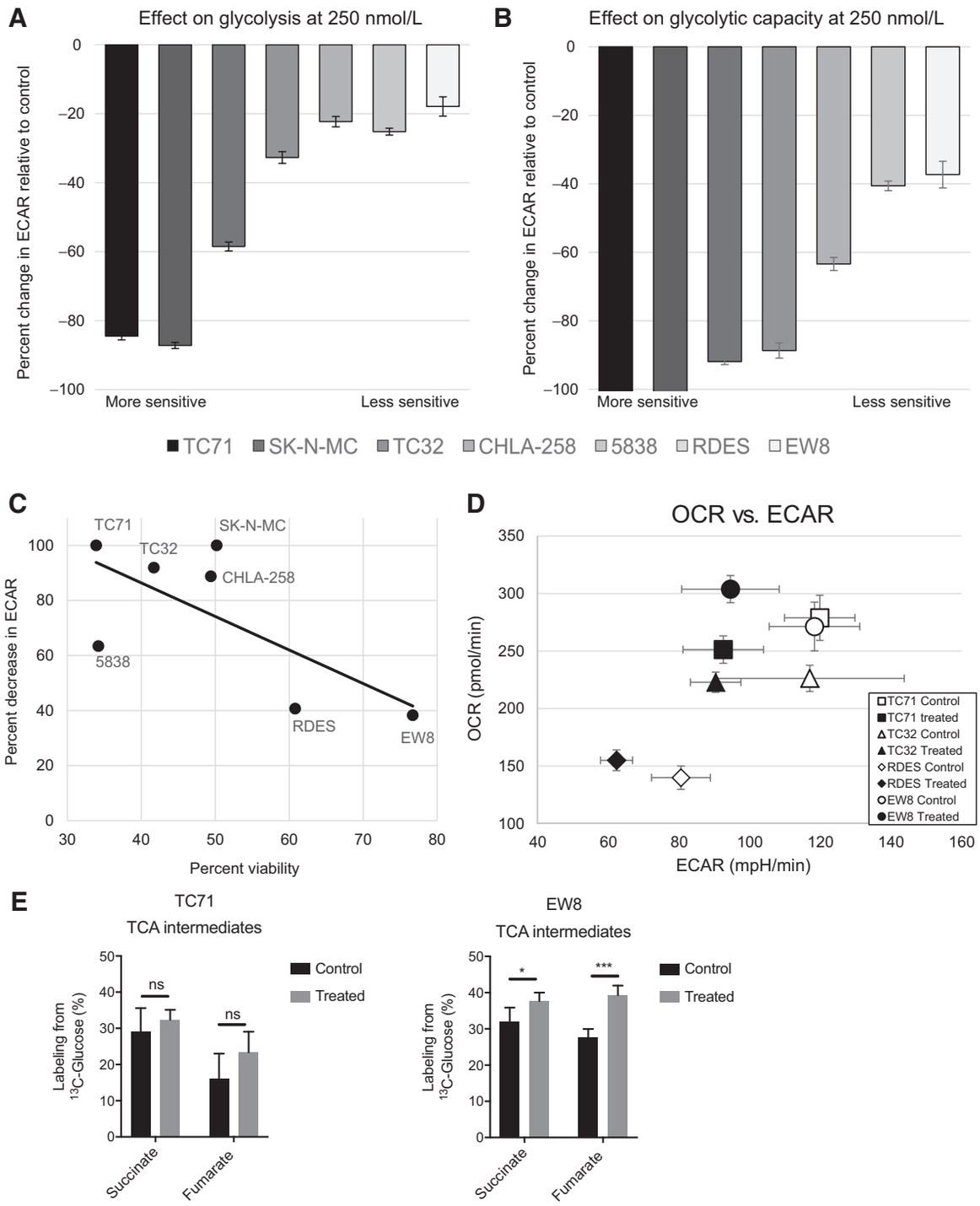

Figure 4.

LDHi sensitivity correlates with cellular bioenergetics. **A** and **B,** Relationship between degree of LDHi effect on glycolysis or glycolytic capacity and Ewing sarcoma cell line sensitivity. Error bars, SEM. Relative cell line sensitivity determined based on experiments in Fig. 1B and Supplementary Fig. S1B. **C,** Pearson correlation between change in ECAR (glycolytic capacity measurement after treatment with 250 nmol/L NCI-737) and cellular viability (as measured by percent inhibition compared with control after treatment with 500 nmol/L NCI-737 using MTT assay). Correlation coefficient = −0.69 with $P = 0.038$. **D,** Energy map of Ewing sarcoma cell lines (TC71, TC32, RDES, and EW8) with and without treatment with 100 nmol/L NCI-737 for 24 hours. Error bars, SD. $P < 0.05$ for comparisons of treated and untreated OCR for EW8, RDES, and TC71 (NS for TC32). $P < 0.01$ for comparisons of treated and untreated ECAR for EW8, RDES, and TC71; $P < 0.05$ for TC32. **E,** Percent ^{13}C incorporation from glucose into major TCA cycle intermediates. *, $P > 0.05$; ***, $P < 0.001$, using t test with Welch correction. ns, nonsignificant.

treated with NCI-737 at 250 nmol/L, TC71 cells underwent an 87% decrease in glycolysis and a 100% decrease in glycolytic capacity, whereas EW8 cells underwent a 19% decrease in glycolysis and a 38% decrease in glycolytic capacity. Notably, cell lines exhibiting larger decreases in glycolysis and glycolytic capacity with drug treatment were more sensitive to the effects of the drug on proliferation, whereas cell lines exhibiting smaller decreases required higher doses of NCI-737 for growth suppression (Fig. 4C). Thus, the magnitude of the biochemical effect of the LDHi on ECAR was predictive of functional response.

In addition, we examined cell lines for potential differences in their use of oxidative phosphorylation, because metabolic plasticity has been shown to affect sensitivity to LDH inhibition (34). To elucidate the relative contributions of the basal rates of glycolysis and oxidative phosphorylation, an energy map of basal and on-treatment ECAR and OCR was generated for several cell lines following 24-hour treatment with NCI-737 at 100 nmol/L (Fig. 4D). Interestingly, although all cell lines experienced an expected decrease in ECAR with treatment, the OCR response varied. The more sensitive cell lines (TC71 and TC32) experienced a relative decrease in OCR, whereas the less sensitive cell lines (RDES and EW8) experienced an increase in OCR, suggesting that increased oxidative phosphorylation may compensate, in part, for the loss of glycolysis in a subset of Ewing sarcoma cell lines, reflecting differences in sensitivity. In addition, data from the *in vitro* study using ^{13}C-labeled glucose revealed a more robust increase of ^{13}C-labeling of TCA cycle intermediates in EW8 compared with TC71 cells, consistent with a greater ability of EW8 cells to redirect pyruvate toward the TCA cycle upon inhibition of LDH (Fig. 4E).

LDH inhibition impairs glycolysis and affects cell survival in aggressive xenograft models of Ewing sarcoma

To evaluate the translational potential of NCI-737 and NCI-006, we treated several orthotopic xenograft models of Ewing sarcoma with the compounds to examine on-target activity, intratumoral drug concentration, toxicity, and efficacy. For all xenograft studies described, treatment was initiated after tumors became palpable. Initial *in vivo* studies were aimed at establishing the optimal route and dose of LDHi in orthotopic xenografts. Oral administration of the agents given at the MTD of 75 mg/kg total daily dose for NCI-737 and 50 mg/kg total daily dose for NCI-006 given for 3 weeks either once or twice daily to mice bearing TC71, TC32, or EW8 tumors resulted in minimal efficacy, although mice in the TC71 and TC32 groups treated with NCI-737 on the twice-daily schedule experienced a slightly decreased tumor growth rate (Supplementary Fig. S9A). Analysis of the effect of the compounds on LDH activity in the tumors revealed an inconsistent pattern of suppression of enzyme activity (Supplementary Fig. S9B). Furthermore, intratumoral drug levels were noted to be variable, establishing that oral dosing was insufficient to achieve adequate intratumoral drug levels and clinically relevant inhibition of LDH in these xenograft models (Supplementary Fig. S9C).

Given the limitations of oral dosing, follow-up studies were performed to evaluate IV dosing in TC71 tumor–bearing mice. NCI-737 was selected for the IV studies due to the slightly more efficacious antitumor effect noted in the oral dosing studies. Initial pilot studies were performed using doses of 25 and 40 mg/kg of NCI-737, given IV on a M/W/F schedule. At 25 mg/kg, no impact on tumor growth rate was observed, and at 40 mg/kg, a minimal change in tumor growth rate was noted (Supplementary Fig. S10A). Samples of plasma and tumor drug levels taken 4 hours after dosing revealed no differences in plasma concentrations (2.9 μmol/L for 25 mg/kg and 2.8 μmol/L for 40 mg/kg) and a slightly greater tumor concentration for the 40 mg/kg group (9 μmol/L vs. 10.3 μmol/L; Supplementary Fig. S10B and S10C). With 25 mg/kg dosing, no inhibition of LDH activity was noted in the tumors 4 hours after dosing; with 40 mg/kg dosing, 60% inhibition of LDH activity was seen at this time-point (Supplementary Fig. S10D).

Based on the lack of LDH inhibition seen at 25 mg/kg and the minimal efficacy observed with the 40 mg/kg dose given on the M/W/F schedule, we next examined doses of 40, 50, and 75 mg/kg given on a more frequent schedule of 5 consecutive days per week by IV to animals bearing TC71 tumors. At these doses, a dose-dependent reduction in tumor growth rates was noted, although the differences did not reach statistical significance (Supplementary Fig. S11A). However, at 75 mg/kg on this schedule, the mice displayed evidence of toxicity, so this dose could not be pursued further.

Pharmacokinetic and pharmacodynamic studies were performed on the animals in the 40 and 50 mg/kg dosing groups after tumor-bearing animals were treated with 3 consecutive days of IV NCI-737. Samples of tumor and plasma drug levels taken 1 hour after dosing revealed average intratumoral concentrations of 12.3 μmol/L (40 mg/kg group) and 18.5 μmol/L (50 mg/kg group) and average plasma concentrations of 8.9 μmol/L (40 mg/kg group) and 11.6 μmol/L (50 mg/kg group). (Fig. 5A; Supplementary Fig. S11B). Pharmacodynamic studies indicated 82% and 93% inhibition of intratumoral LDH activity in the 40 mg/kg and 50 mg/kg groups, respectively (Fig. 5B). Notably, intratumoral drug concentration and LDH inhibition rapidly diminished over a short interval. When animals treated at the same doses underwent tumor sampling 4 hours after dose (vs. 1 hour), a rapid loss (28%) of intratumoral compound and a corresponding decrease in the degree of LDH inhibition (82% to 58%) were observed between the 1- and 4-hour sampling times (Fig. 5C and D). These data were consistent with the known pharmacologic properties and full pharmacokinetic profile of NCI-737, which indicate a half-life of approximately 5 hours in plasma.

Given the rapid loss of LDH inhibition in the tumor, we hypothesized that the tumor growth response might be blunted due to inability to maintain continuous inhibition of tumor LDH on the 5 days/week schedule. To test this hypothesis, we evaluated a continuous 7 days/week dosing schedule. A daily dose of 60 mg/kg was chosen to attempt to minimize toxicity and maximize efficacy. NCI-737 treatment for 7 days/week resulted in statistically significant tumor growth suppression in mice bearing TC71 xenografts (Fig. 6A). In addition, histopathologic analysis of tumors revealed that treated tumors had a nearly 2-fold increase in necrosis over vehicle-treated tumors (59% vs. 33%). Similarly, tumors from EW8-bearing xenografts treated with NCI-737 at 60 mg/kg displayed a statistically significant increase in necrosis compared with control (43% vs. 28%; Fig. 6B and C; Supplementary Fig. S12A). However, treatment at this dose was not sufficient to affect overall tumor growth in the EW8 model, suggesting that the relative sensitivity differences noted *in vitro* may be relevant *in vivo* (Supplementary Fig. S12B).

Finally, to confirm the *in vivo* on-target activity of the LDHi, we performed hyperpolarized MR spectroscopy, using hyperpolarized ^{13}C-pyruvate, of orthotopic xenograft Ewing sarcoma tumors in mice to quantify the ratio of ^{13}C-lactate generated from ^{13}C-pyruvate 30 minutes after a single IV dose of NCI-737 at

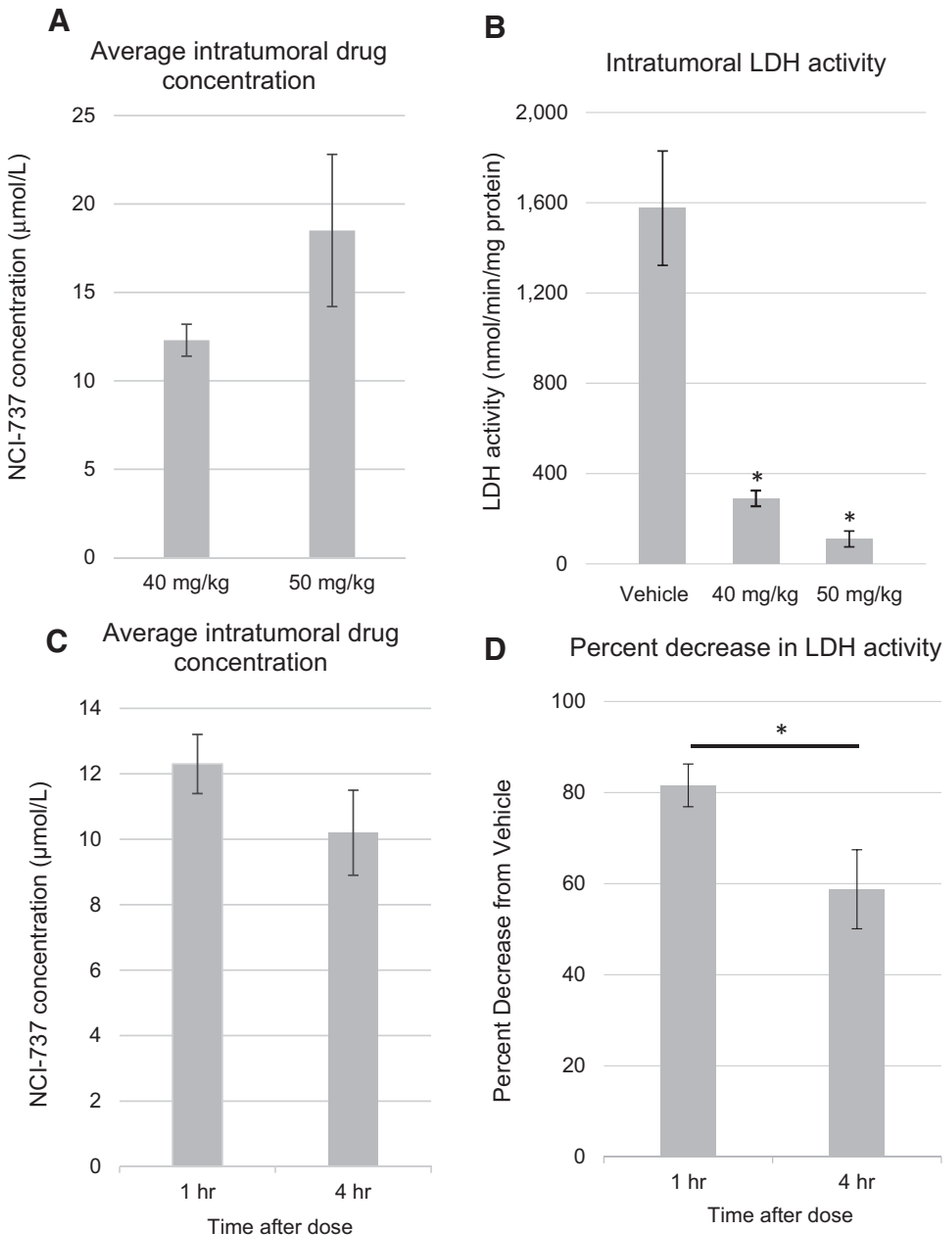

Figure 5.
LDHi have a dose- and time-dependent effect on tumor cell LDH activity *in vivo*. **A,** Average intratumoral drug concentrations 1 hour after dosing of NCI-737 on day 3 in TC71-bearing xenografts ($n = 3$ mice/group). **B,** Intratumoral LDH activity 1 hour after dosing of NCI-737 on day 3 in TC71-bearing xenografts ($n = 3$ mice/group). *, $P < 0.05$, compared with vehicle. **C,** Average intratumoral drug concentrations after 1 and 4 hours following treatment with NCI-737 at 40 mg/kg in TC71-bearing xenografts ($n = 3$ mice/group). **D,** Percent change in intratumoral LDH activity after 1 and 4 hours following treatment with NCI-737 at 40 mg/kg in TC71-bearing xenografts ($n = 3$ mice/group). *, $P < 0.05$ between groups.

the efficacious dose of 60 mg/kg. NCI-737 treatment resulted in a 57% and 49% reduction in the labeled lactate/pyruvate ratio in TC71 and EW8 tumors, respectively (Fig. 6D; Supplementary Fig. S13). Taken together, these findings verified the on-target activity of the agent *in vivo* and were consistent with the *in vitro* results. Furthermore, the *in vivo* data indicate that to achieve tumor growth inhibition, sustained inhibition of LDH through frequent dosing at the highest tolerable dose is required.

Hemolysis is the primary dose-limiting toxicity of LDH inhibition

Assessments of toxicity via observations of general appearance, blood parameters, and necropsy were performed on animals treated via a 5 days/week IV dosing schedule with NCI-737 at 40, 50, or 75 mg/kg. Toxicity assessments were performed at day 3 and at tumor or humane endpoint. Although mice tolerated treatments without weight loss (Supplementary Fig. S14A), a dose-dependent intolerance of NCI-737 was noted. All mice treated at 40 mg/kg displayed no toxicity, whereas 1 of 3 mice treated at 50 mg/kg and 2 of 3 mice treated at 75 mg/kg displayed decreased physical activity by day 2 of treatment. Laboratory and pathologic assessments of all mice revealed that hemolysis was the primary dose-limiting toxicity observed, with a dose-dependent decrease in hemoglobin noted within 3 days of starting treatment (Supplementary Fig. S14B). Within 3 days, hemoglobin values began to fall below the lower limit of the normal range of 11 g/dL in mice receiving the lowest (40 mg/kg) dose. At higher doses, hemoglobin values were below 8 g/dL. By endpoint,

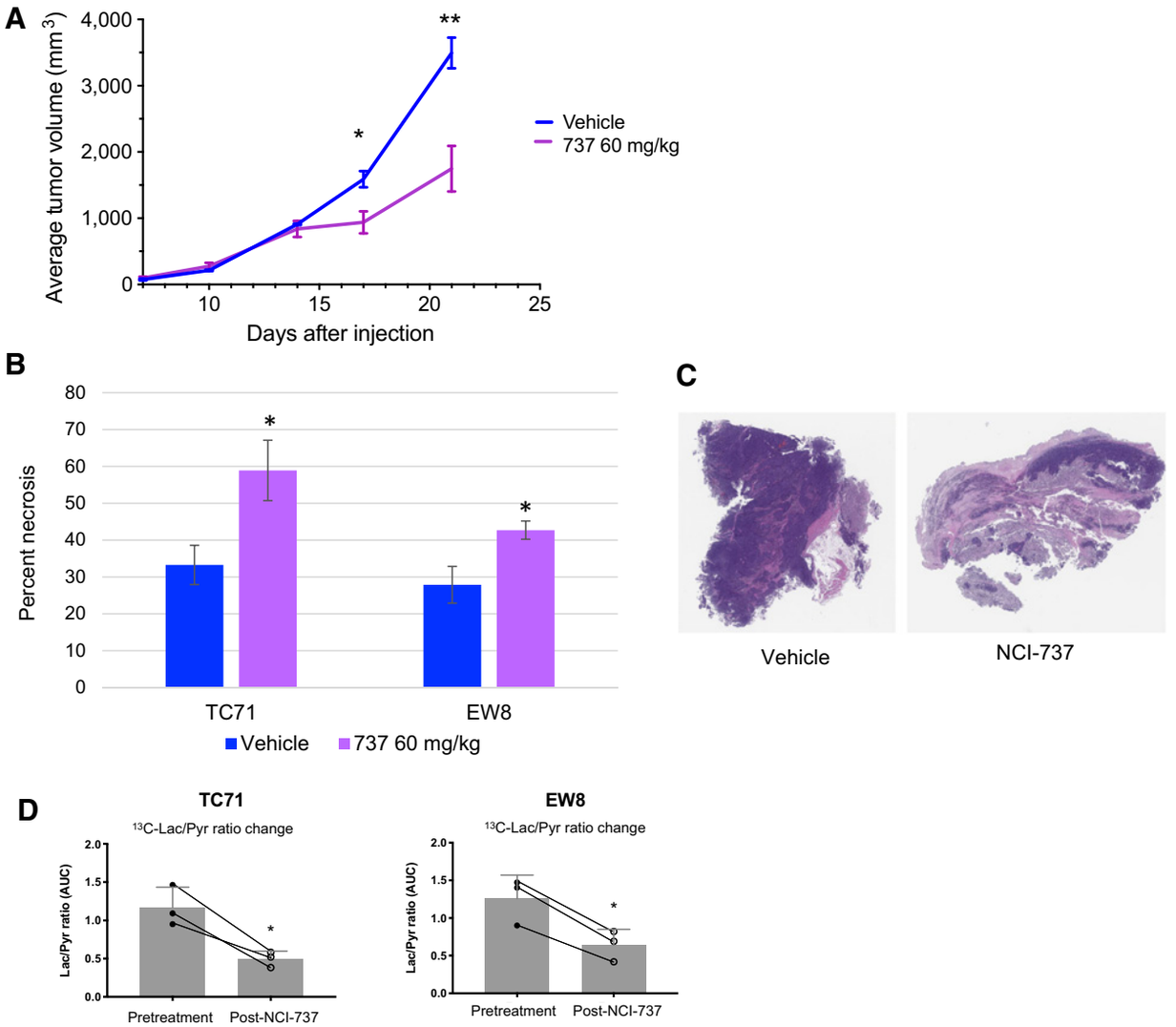

Figure 6.

LDH inhibition impairs glycolysis and affects cell survival *in vivo*. **A,** Tumor growth curves for TC71-bearing xenografts treated 7 days per week with IV NCI-737 at 60 mg/kg ($n = 5$ mice/group). Error bars, SEM. *P* values, as compared with vehicle: *, $P < 0.05$; **, $P < 0.01$. **B,** Percent necrosis in tumor tissue of TC71- and EW8-bearing xenografts treated with IV NCI-737 on a 7-day per week schedule ($n = 5$ mice/group). Error bars, SEM. *, $P < 0.05$, for comparison between vehicle and treated tumors. **C,** Representative hematoxylin and eosin–stained whole slide digital images of entire tumor sections resected from TC71-bearing xenografts treated with vehicle (left) or NCI-737 (right). Viable tissue is shown in dark purple. Visual image analysis can be found in Supplementary Fig. S12A. **D,** ^{13}C lactate to pyruvate ratio change 30 minutes after injection of NCI-737 at 60 mg/kg in xenografted TC71 and EW8 tumors ($n = 3$ mice/group). Lines indicate changes in each animal. *, $P < 0.05$ comparing pre- and posttreatment animals.

average hemoglobin levels had decreased further to 9.1, 4.6, and 5.3 g/dL in the 40, 50, and 75 mg/kg treated groups, respectively, indicating that toxicity was cumulative with continued dosing.

A corresponding rise in total bilirubin was also noted both at day 3 of treatment and at endpoint (Supplementary Fig. S14C). Although measurements of direct bilirubin were not obtained, normal liver studies were noted in all mice, suggesting that the rise in total bilirubin was the result of an increase in the indirect bilirubin fraction, which is consistent with red blood cell breakdown. In addition, mice treated at all dose levels were noted to have an increase in splenic weight at endpoint, further supporting hemolysis as the major toxicity (Supplementary Fig. S14D). Red blood cells lack nuclei and mitochondria and therefore rely entirely on glycolysis for bioenergetics (35). A previous study describing the phenotypes associated with genetic loss of LDHA in murine models reported nonlethal hemolytic anemia as a main finding, supporting the idea that this toxicity is on-target (4). Of note, no other lab abnormalities were seen on complete blood counts or chemistry panels performed as part of the toxicity assessment.

Discussion

In this study, we have demonstrated that Ewing sarcoma cells display a marked dependency on LDHA, due, in part, to the

regulation of *LDHA* by the oncogenic transcription factor EWS-FLI1. We have shown that genetic or pharmacologic inhibition of LDHA reduces proliferation and induces apoptosis in Ewing sarcoma cells, and that this is associated with suppression of glycolytic flux and perturbation of the NADH/NAD^+ ratio. In addition, we have explored the translational potential of this target through *in vivo* characterization of two novel LDHi, performing analyses of drug delivery routes, pharmacokinetics, pharmacodynamics, toxicity, and efficacy.

We show that LDHA is an important enzyme for the survival of Ewing sarcoma cells, which are remarkably sensitive to both genetic and pharmacologic inhibition of LDH. Pharmacologic targeting of LDH using NCI-737 and NCI-006 inhibited proliferation of Ewing sarcoma cells both *in vitro* and *in vivo* through inhibition of glycolysis and induction of apoptosis. This finding is consistent with published literature describing targeting of LDH in other sensitive cancer types (9, 36). Notably, the effect of these agents on proliferation of Ewing sarcoma cells exceeded the effects seen on other types of cancer cells. Our work suggests that the biology of Ewing sarcoma, in particular the presence of the driving *EWS-FLI1* fusion oncogene (17, 18), contributes to the sensitivity of these cells to glycolytic inhibition. Specifically, we have shown that the EWS-FLI1 fusion oncoprotein directly regulates LDHA, but not LDHB, expression. This finding is supported by the recent report that EWS-FLI1 regulates metabolic pathways in Ewing sarcoma, where it shifts glucose consumption away from oxidative metabolism and toward glycolysis (30), and by evidence that Ewing sarcoma cells are highly glycolytic and highly susceptible to glucose deprivation and disruption of glucose metabolism (31, 37–40). In addition, there are clinical data to suggest that outcomes for Ewing sarcoma patients are worse for those who exhibit higher plasma levels of LDH (41–43).

The metabolic consequences of NCI-737 and NCI-006 on Ewing sarcoma were suppressed glycolytic flux through inhibition of the conversion of pyruvate to lactate, which was observed in both *in vitro* and *in vivo* models, concomitant with disruption of the NAD^+/NADH ratio. By extracellular flux analysis, NCI-737 treatment resulted in decreased ECAR, the magnitude of which was predictive of the effect on cellular viability across multiple Ewing sarcoma cell lines. The ability of the cells to engage oxidative phosphorylation through the TCA cycle, which has been reported as a resistance mechanism in other cancer types (7, 34), also emerged as a potential factor contributing to differential sensitivity to LDHi.

Given the critical need for novel therapies for patients with Ewing sarcoma (19–21), the remainder of our work was focused on determining the translational potential of LDHi for this disease. Although suppression of glycolysis was profound in the single treatment MR spectroscopy experiments, the long-term *in vivo* studies revealed that effect on xenograft tumor growth was dependent on achievement of consistently high and sustained levels of the inhibitors intratumorally, which required frequent IV dosing. This requirement may also explain why a maximal intratumoral drug concentration in the micromolar range could result in less antitumor activity than would be expected based on the *in vitro* dosing range. Although an increase in the delivered dose or a more frequent dosing interval may have been able to overcome this, the on-target dose-dependent hemolytic anemia observed in the mice limited further dose-escalation. Thus, there appears to be a narrow therapeutic window for these LDHi to move forward into clinical development as single agents. Strategies to overcome these challenges include development of novel delivery methods for LDHi, or combinatorial approaches that might allow for lower doses of LDHi to be effective. Based on published data, kinase inhibitors, HSP90 inhibitors, oxidative phosphorylation inhibitors, and inducers of reactive oxygen species represent several potential combination partners worthy of further study (5, 44–47). In conclusion, our findings suggest that further translational preclinical work is necessary to optimize the potential of LDHi as anticancer agents, but that due to their exquisite sensitivity to glycolytic impairment, Ewing sarcoma may be one of the best indications for their use.

Disclosure of Potential Conflicts of Interest

No potential conflicts of interest were disclosed.

Disclaimer

The content of this publication does not necessarily reflect the views or policies of the Department of Health and Human Services, nor does mention of trade names, commercial products, or organizations imply endorsement by the U.S. Government.

Authors' Contributions

Conception and design: C. Yeung, A.E. Gibson, S.H. Issaq, A. Mendoza, L.J. Helman, V. Darley-Usmar, L.M. Neckers, C.M. Heske

Development of methodology: C. Yeung, A.E. Gibson, S.H. Issaq, J.T. Baumgart, D.J. Urban, G.A. Benavides, G.L. Squadrito, T. Dowdy, V. Darley-Usmar, L.M. Neckers, C.M. Heske

Acquisition of data (provided animals, acquired and managed patients, provided facilities, etc.): C. Yeung, A.E. Gibson, S.H. Issaq, N. Oshima, J.T. Baumgart, D.J. Urban, M.S. Johnson, G.A. Benavides, S. Eldridge, T. Dowdy, V. Ruiz-Rodado, A. Mendoza, J.F. Shern, G.M. Stott, M.C. Krishna, M.D. Hall, C.M. Heske

Analysis and interpretation of data (e.g., statistical analysis, biostatistics, computational analysis): C. Yeung, A.E. Gibson, S.H. Issaq, N. Oshima, J.T. Baumgart, D.J. Urban, M.S. Johnson, G.A. Benavides, G.L. Squadrito, M.E. Yohe, H. Lei, S. Eldridge, J. Hamre III, T. Dowdy, V. Ruiz-Rodado, A. Lita, A. Mendoza, J.F. Shern, M. Larion, L.J. Helman, G.M. Stott, M.D. Hall, V. Darley-Usmar, L.M. Neckers, C.M. Heske

Writing, review, and/or revision of the manuscript: C. Yeung, A.E. Gibson, S.H. Issaq, J.T. Baumgart, G. Rai, D.J. Urban, M.S. Johnson, G.A. Benavides, G.L. Squadrito, M.E. Yohe, V. Ruiz-Rodado, A. Lita, J.F. Shern, M. Larion, L.J. Helman, M.D. Hall, V. Darley-Usmar, L.M. Neckers, C.M. Heske

Administrative, technical, or material support (i.e., reporting or organizing data, constructing databases): S.H. Issaq, L.D. Edessa, G.L. Squadrito, T. Dowdy, A. Mendoza, G.M. Stott, C.M. Heske

Study supervision: C. Yeung, M.D. Hall, V. Darley-Usmar, C.M. Heske

Other (conception, design, and synthesis of the inhibitors used in this study): G. Rai

Other (I performed the computational analysis for quantifying percent necrosis in the tumors and wrote the M&M for that specific part only): J. Hamre III

Acknowledgments

Authors were supported by grants from the Intramural Research Program of the NIH as follows: C. Yeung, A.E. Gibson, S.H. Issaq, N. Oshima, J.T. Baumgart, L.D. Edessa, M.E. Yohe, H. Lei, T. Dowdy, V. Ruiz-Rodado, A. Lita, A. Mendoza, J.F. Shern, M. Larion, L.J. Helman, M.C. Krishna, L.M. Neckers, and C.M. Heske. N. Oshima, J.T. Baumgart, D.J. Urban, M.S. Johnson, G.A. Benavides, G.L. Squadrito, M.E. Yohe, H. Lei, S. Eldridge, J. Hamre III, T. Dowdy, V. Ruiz-Rodado, A. Lita, A. Mendoza, J.F. Shern, M. Larion, L.J. Helman, G.M. Stott, M.D. Hall, V. Darley-Usmar, L.M. Neckers, and C.M. Heske were supported by the NCI, Center for Cancer Research; G. Rai, D.J. Urban, and M.D. Hall were supported by the National Center for Advancing Translational Sciences; S. Eldridge was supported by the Developmental Therapeutics Program, Division of Cancer Treatment and Diagnosis. This project has also been funded in part with Federal funds from the NCI, NIH, under Contract No. HHSN261200800001E (J. Hamre III and G.M. Stott) and with funding

from the Chemical Biology Consortium, NCI Experimental Therapeutics (NExT) Program (N. Oshima, G. Rai, D.J. Urban, M.S. Johnson, G.A. Benavides, G.L. Squadrito, S. Eldridge, M.C. Krishna, M.D. Hall, V. Darley-Usmar, and L.M. Neckers).

The authors would like to thank Devorah Gallardo, Rebekah Madrid, Dr. Daniel Crooks, Kristin Beebe, Dr. David Venzon, and Matilda Culp for their assistance with this study.

The costs of publication of this article were defrayed in part by the payment of page charges. This article must therefore be hereby marked *advertisement* in accordance with 18 U.S.C. Section 1734 solely to indicate this fact.

Received February 16, 2019; revised June 26, 2019; accepted August 12, 2019; published first August 20, 2019.

References

1. Warburg O, Wind F, Negelein E. The metabolism of tumors in the body. J Gen Physiol 1927;8:519–30.
2. Zhao Y, Liu H, Riker AI, Fodstad O, Ledoux SP, Wilson GL, et al. Emerging metabolic targets in cancer therapy. Front Biosci (Landmark Ed) 2011;16: 1844–60.
3. Koppenol WH, Bounds PL, Dang CV. Otto Warburg's contributions to current concepts of cancer metabolism. Nat Rev Cancer 2011;11:325–37.
4. Xie H, Hanai J, Ren JG, Kats L, Burgess K, Bhargava P, et al. Targeting lactate dehydrogenase–a inhibits tumorigenesis and tumor progression in mouse models of lung cancer and impacts tumor-initiating cells. Cell Metab 2014; 19:795–809.
5. Le A, Cooper CR, Gouw AM, Dinavahi R, Maitra A, Deck LM, et al. Inhibition of lactate dehydrogenase A induces oxidative stress and inhibits tumor progression. Proc Natl Acad Sci U S A 2010;107:2037–42.
6. Sheng SL, Liu JJ, Dai YH, Sun XG, Xiong XP, Huang G. Knockdown of lactate dehydrogenase A suppresses tumor growth and metastasis of human hepatocellular carcinoma. FEBS J 2012;279:3898–910.
7. Fantin VR, St-Pierre J, Leder P. Attenuation of LDH-A expression uncovers a link between glycolysis, mitochondrial physiology, and tumor maintenance. Cancer Cell 2006;9:425–34.
8. Zhao YH, Zhou M, Liu H, Ding Y, Khong HT, Yu D, et al. Upregulation of lactate dehydrogenase A by ErbB2 through heat shock factor 1 promotes breast cancer cell glycolysis and growth. Oncogene 2009;28:3689–701.
9. Rong Y, Wu W, Ni X, Kuang T, Jin D, Wang D, et al. Lactate dehydrogenase A is overexpressed in pancreatic cancer and promotes the growth of pancreatic cancer cells. Tumour Biol 2013;34:1523–30.
10. Doherty JR, Cleveland JL.Targeting lactate metabolism for cancer therapeutics. J Clin Invest 2013;123:3685–92.
11. Miao P, Sheng S, Sun X, Liu J, Huang G. Lactate dehydrogenase A in cancer: a promising target for diagnosis and therapy. IUBMB Life 2013;65:904–10.
12. Ward RA, Brassington C, Breeze AL, Caputo A, Critchlow S, Davies G, et al. Design and synthesis of novel lactate dehydrogenase A inhibitors by fragment-based lead generation. J Med Chem 2012;55:3285–306.
13. Dragovich PS, Fauber BP, Corson LB, Ding CZ, Eigenbrot C, Ge H, et al. Identification of substituted 2-thio-6-oxo-1,6-dihydropyrimidines as inhibitors of human lactate dehydrogenase. Bioorg Med Chem Lett 2013;23: 3186–94.
14. Kohlmann A, Zech SG, Li F, Zhou T, Squillace RM, Commodore L, et al. Fragment growing and linking lead to novel nanomolar lactate dehydrogenase inhibitors. J Med Chem 2013;56:1023–40.
15. Rai G, Brimacombe KR, Mott BT, Urban DJ, Hu X, Yang SM, et al. Discovery and optimization of potent, cell-active pyrazole-based inhibitors of lactate dehydrogenase (LDH). J Med Chem 2017;60:9184–204.
16. Balamuth NJ, Womer RB. Ewing's sarcoma. Lancet Oncol 2010;11:184–92.
17. May WA, Gishizky ML, Lessnick SL, Lunsford LB, Lewis BC, Delattre O, et al. Ewing sarcoma 11;22 translocation produces a chimeric transcription factor that requires the DNA-binding domain encoded by FLI1 for transformation. Proc Natl Acad Sci U S A 1993;90:5752–6.
18. Delattre O, Zucman J, Plougastel B, Desmaze C, Melot T, Peter M, et al. Gene fusion with an ETS DNA-binding domain caused by chromosome translocation in human tumours. Nature 1992;359:162–5.
19. Fidler MM, Frobisher C, Guha J, Wong K, Kelly J, Winter DL, et al. Long-term adverse outcomes in survivors of childhood bone sarcoma: the British Childhood Cancer Survivor Study. Br J Cancer 2015;112:1857–65.
20. Hamilton SN, Carlson R, Hasan H, Rassekh SR, Goddard K. Long-term outcomes and complications in pediatric ewing sarcoma. Am J Clin Oncol 2015;40:423–28.
21. Marina NM, Liu Q, Donaldson SS, Sklar CA, Armstrong GT, Oeffinger KC, et al. Longitudinal follow-up of adult survivors of Ewing sarcoma: a report from the childhood cancer survivor study. Cancer 2017;123:2551–60.
22. Heske CM, Mendoza A, Edessa LD, Baumgart JT, Lee S, Trepel J, et al. STA-8666, a novel HSP90 inhibitor/SN-38 drug conjugate, causes complete tumor regression in preclinical mouse models of pediatric sarcoma. Oncotarget 2016;7:65540–52.
23. Gryder BE, Yohe ME, Chou HC, Zhang X, Marques J, Wachtel M, et al. PAX3-FOXO1 establishes myogenic super enhancers and confers BET bromodomain vulnerability. Cancer Discov 2017;7:884–99.
24. Issaq SH, Teicher BA, Monks A. Bioenergetic properties of human sarcoma cells help define sensitivity to metabolic inhibitors. Cell Cycle 2014;13: 1152–61.
25. Hill BG, Benavides GA, Lancaster JR Jr., Ballinger S, Dell'Italia L, Jianhua Z, et al. Integration of cellular bioenergetics with mitochondrial quality control and autophagy. Biol Chem 2012;393:1485–512.
26. Ruiz-Rodado V, Lita A, Dowdy T, Celiku O, Cavazos-Saldana A, Wang H, et al. Metabolic plasticity of IDH1- mutant glioma cell lines is responsible for low sensitivity to glutaminase inhibition. Cell Reports-D-19-018192019. Available from: https://ssrn.com/abstract=3387658.
27. Saito K, Matsumoto S, Takakusagi Y, Matsuo M, Morris HD, Lizak MJ, et al. 13C-MR spectroscopic imaging with hyperpolarized [1-13C]pyruvate detects early response to radiotherapy in SCC Tumors and HT-29 Tumors. Clin Cancer Res 2015;21:5073–81.
28. Lawlor ER, Sorensen PH. Twenty years on: what do we really know about ewing sarcoma and what is the path forward? Crit Rev Oncog 2015;20: 155–71.
29. Kovar H. Blocking the road, stopping the engine or killing the driver? Advances in targeting EWS/FLI-1 fusion in Ewing sarcoma as novel therapy. Expert Opin Ther Targets 2014;18:1315–28.
30. Tanner JM, Bensard C, Wei P, Krah NM, Schell JC, Gardiner J, et al. EWS/FLI is a master regulator of metabolic reprogramming in ewing sarcoma. Mol Cancer Res 2017;15:1517–30.
31. Mutz CN, Schwentner R, Aryee DN, Bouchard ED, Mejia EM, Hatch GM, et al. EWS-FLI1 confers exquisite sensitivity to NAMPT inhibition in Ewing sarcoma cells. Oncotarget 2017;8:24679–93.
32. Riggi N, Knoechel B, Gillespie SM, Rheinbay E, Boulay G, Suva ML, et al. EWS-FLI1 utilizes divergent chromatin remodeling mechanisms to directly activate or repress enhancer elements in Ewing sarcoma. Cancer Cell 2014; 26:668–81.
33. Sheffield NC, Pierron G, Klughammer J, Datlinger P, Schonegger A, Schuster M, et al. DNA methylation heterogeneity defines a disease spectrum in Ewing sarcoma. Nat Med 2017;23:386–95.
34. Boudreau A, Purkey HE, Hitz A, Robarge K, Peterson D, Labadie S, et al. Metabolic plasticity underpins innate and acquired resistance to LDHA inhibition. Nat Chem Biol 2016;12:779–86.
35. van Wijk R, van Solinge WW. The energy-less red blood cell is lost: erythrocyte enzyme abnormalities of glycolysis. Blood 2005;106: 4034–42.
36. Yao F, Zhao T, Zhong C, Zhu J, Zhao H. LDHA is necessary for the tumorigenicity of esophageal squamous cell carcinoma. Tumour Biol 2013;34:25–31.
37. Dasgupta A, Trucco M, Rainusso N, Bernardi RJ, Shuck R, Kurenbekova L, et al. Metabolic modulation of Ewing sarcoma cells inhibits tumor growth and stem cell properties. Oncotarget 2017;8:77292–308.
38. Heske CM, Davis MI, Baumgart JT, Wilson KM, Gormally MV, Chen L, et al. Matrix screen identifies synergistic combination of PARP inhibitors and nicotinamide phosphoribosyltransferase (NAMPT) inhibitors in Ewing sarcoma. Clin Cancer Res 2017;23:7301–11.
39. Sanchez-Sanchez AM, Antolin I, Puente-Moncada N, Suarez S, Gomez-Lobo M, Rodriguez C, et al. Melatonin cytotoxicity is associated to warburg effect inhibition in ewing sarcoma cells. PLoS One 2015;10: e0135420.

40. Issaq SH, Mendoza A, Fox SD, Helman LJ. Glutamine synthetase is necessary for sarcoma adaptation to glutamine deprivation and tumor growth. Oncogenesis 2019;8:20.
41. Bacci G, Ferrari S, Longhi A, Rimondini S, Versari M, Zanone A, et al. Prognostic significance of serum LDH in Ewing's sarcoma of bone. Oncol Rep 1999;6:807–11.
42. Li S, Yang Q, Wang H, Wang Z, Zuo D, Cai Z, et al. Prognostic significance of serum lactate dehydrogenase levels in Ewing's sarcoma: a meta-analysis. Mol Clin Oncol 2016;5:832–8.
43. Palmerini E, Jones RL, Setola E, Picci P, Marchesi E, Luksch R, et al. Irinotecan and temozolomide in recurrent Ewing sarcoma: an analysis in 51 adult and pediatric patients. Acta Oncol 2018;57:958–64.
44. Fu J, Jiang H, Wu C, Jiang Y, Xiao L, Tian Y. Overcoming cetuximab resistance in Ewing's sarcoma by inhibiting lactate dehydrogenase-A. Mol Med Rep 2016;14:995–1001.
45. Manerba M, Di Ianni L, Govoni M, Roberti M, Recanatini M, Di Stefano G. LDH inhibition impacts on heat shock response and induces senescence of hepatocellular carcinoma cells. Eur J Pharm Sci 2017;105:91–8.
46. Vangapandu HV, Alston B, Morse J, Ayres ML, Wierda WG, Keating MJ, et al. Biological and metabolic effects of IACS-010759, an OxPhos inhibitor, on chronic lymphocytic leukemia cells. Oncotarget 2018;9:24980–91.
47. Molina JR, Sun Y, Protopopova M, Gera S, Bandi M, Bristow C, et al. An inhibitor of oxidative phosphorylation exploits cancer vulnerability. Nat Med 2018;24:1036–46.